HHS Public Access

Author manuscript

Exp Eye Res. Author manuscript; available in PMC 2023 May 23.

Published in final edited form as:

Exp Eye Res. 2023 January ; 226: 109341. doi:10.1016/j.exer.2022.109341.

+Effects of experimental glaucoma in *Lama1*^{nmf223} mutant mice

Salaheddine Madhoun[A], **Manuela Tosi Comelis Martins**[A], **Arina Korneva**[A], **Thomas V Johnson**[A], **Elizabeth Kimball**[A], **Sarah Quillen**[A], **Mary Ellen Pease**[A], **Malia Edwards**[B], **Harry Quigley**[A]

[A]Glaucoma Center of Excellence, Wilmer Eye Institute, Johns Hopkins University, Baltimore, Maryland, United States of America

[B]Wilmer Eye Institute, Johns Hopkins School of Medicine, Baltimore, Maryland, United States of America

Abstract

To identify changes in response to experimental intraocular pressure (IOP) elevation associated with the *laminin α1* nmf223 mutation in mice.

Laminin mutant (LM) mice (*Lama1*^{nmf223}) and C57BL/6J (B6) mice in two age groups each (4-5 months and >1 year) underwent intracameral microbead injections to produce unilaterally elevated IOP. We assessed axonal transport block of immunofluorescently labeled amyloid precursor protein (APP) after 3 days and retinal ganglion cell (RGC) axon loss after 6 weeks. Light, electron and fluorescent microscopy was used to study baseline anatomic differences and effects of 3-day IOP elevation in younger LM mice.

In younger mice of both LM and B6 strains, elevated IOP led to increased APP block in the retina, prelaminar optic nerve head (preONH), unmyelinated optic nerve (UON), and myelinated optic nerve (MON). APP blockade not significantly different between younger B6 and LM mouse strains. Older LM mice had greater APP accumulation in both control and glaucoma eyes compared to older B6, however, accumulation was not significantly greater in LM glaucoma eyes compared to LM controls. Axon loss at 6 weeks was 12.2% in younger LM and 18.7% in younger B6 mice (difference between strains, $p = 0.22$, Mann Whitney test). Untreated LM optic nerve area was lower compared to B6 (nerve area, $p < 0.0001$, t-test). Aberrant axon bundles, as well as defects, thickening and reduplication of pia mater, were seen in the optic nerves of younger LM mice.

Axonal transport blockade significantly differed between old B6 and old LM mice in control and glaucoma eyes, and younger LM mice had abnormal axon paths and lower optic nerve area.

Keywords

glaucoma; mouse; optic nerve head; axonal transport; amyloid precursor protein; axon; laminin

Corresponding author: Salaheddine Madhoun, 400 N Broadway, Baltimore, MD, 21231, USA. msalahe1@jhu.edu Phone: 410-955-3337.

Declarations of interest: none.

1.1 Introduction

Glaucoma damage to retinal ganglion cell axons is related to axonal transport blockade at the optic nerve head (ONH) in human (Quigley et al, 1981) and monkey (Quigley and Addicks, 1980) eyes and in the corresponding unmyelinated optic nerve (UON) region in mice (Howell et al, 2007). A major cause of RGC injury and death is IOP-generated mechanical stress, manifesting both as hoop stress on the ONH at the peripapillary sclera (PPS) and as the translaminar pressure difference between IOP and optic nerve (ON) tissue pressure (Quigley, 2016). The extracellular fiber structure and orientation, as well as the cellular orientation of the PPS and ONH are designed to withstand these stresses. Collagen and elastic fibers in the PPS are arranged circumferentially around the ONH in mammalian eyes (Quigley et al, 1991; Gelman et al, 2010; Pijanka et al, 2015). Astrocytes make up the rodent lamina cribrosa (LC) (Sun et al, 2009), which is largely cellular, while the eyes of larger mammals have astrocyte-covered connective tissue beams comprising the LC. Both the astrocytic LC of mice and rats, and the beams of larger animal LC, are arrayed directly across the ONH from one side to the other (Jones, 2015). Mouse astrocytes are stretched across the ONH attached to their basement membrane at the PPS.

The extracellular matrix (ECM) of the primate ONH contains collagen types I and III, elastin, and glycosaminoglycans in the LC beams, while in mice and rats these molecules are arrayed in the PPS (Morrison et al, 1989). Collagen IV and laminin are key elements of astrocytic basement membranes. Laminins are glycoproteins consisting of heterotrimers of 15 isoforms, each containing one of the five α chains, one of 3 β chains, and one of 3 γ chains. Laminins serve varied functions, particularly forming an essential element of the attachment between cells and their basement membrane (Colognato and Yurchenco, 2000). In the mouse and human eye, laminin α1 is produced as a key portion of the internal limiting membrane (ILM), pia mater, lens, and ciliary body (Falk et al, 1999; Kohno et al, 1987).

Astrocytes link to basement membranes through the integrin family of membrane-spanning proteins, activating intracellular signaling pathways including sensation of mechanical stress (Zhong et al, 2013). Integrins are heterodimers of α and β subunits, with specific heterodimer combinations determining ligand specificity and intracellular responses. In normal primate eyes, integrin dimers in astrocytes (Hernandez, 2000; Morrison, 2006) include subtypes with affinity for attachment to laminin. Defects in astrocyte attachment to their basement membrane at the PPS were recognized as an important pathological step in experimental mouse glaucoma (Quillen et al, 2020). Thus, molecular changes in laminin structure could alter the glial respsonse to IOP elevation in experimental glaucoma models.

Edwards et al. described ocular findings in the retina of mice with a missense mutation in laminin α1 (*Lama1*^{nmf223}), wherein cysteine substitutes for tyrosine at amino acid 265 within the highly conserved laminin N-terminal domain, which is critical for laminin polymerization (Edwards et al, 2009). They identified defects in the ILM and malpositioning of retinal blood vessels resulting from ectopic migration of retinal glia into the vitreous cavity during development. While laminin α1 was present in the ILM and other basement membranes, their structural integrity was compromised. It was suggested that this mutation disrupts the binding of laminin α1 by retinal Müller glia. Johnson et al. exploited the ILM

lack of continuity in these mutants to provide access to retina for intravitreally injected stem cell-derived neurons (Zhang and Johnson, 2021). We identified defects in laminin distribution in the optic nerve region of *Lama1*^{nmf223} mice and hypothesize that this may provide information on the role of integrin-linked laminin connections in axonal transport blockade and neuronal death in rodent glaucoma.

Methods

2.1 Animal Groups and Treatments:

All animals (N=66, Mice; N=132, eyes) were treated in accordance with the ARVO Statement for the Use of Animals in Ophthalmic and Vision Research, using protocols approved and monitored by the Johns Hopkins University School of Medicine Animal Care and Use Committee. Two strains were used at 2 ages each. These were C57BL/6J mice (B6, Jackson Laboratory, Bar Harbor, Maine), denoted younger B6 (YB6) and older B6 (OB6), and laminin mutant mice received from Dr. Malia Edwards (Wilmer Eye Institute, C57BL/6J-Lama1^{nmf223}/J), denoted younger laminin mutant (YLM) and older laminin mutant (OLM). Younger group mice of both strains were 4-5 months old, and older group mice were 12-14 months old.

2.2 Microbead Injections:

Animals (N=65, Mice; N=130, eyes) received unilateral intracameral microbead injection to induce experimental IOP elevation (Cone et al, 2012, 2020). Of the mice that received bead injections, 33 were part of the 3-day glaucoma model used in the APP analysis, 32 were part of the 6-week glaucoma model used in optic nerve counts. Mice were anesthetized with intraperitoneal ketamine (50 mg/kg), xylazine (10 mg/kg), and acepromazine (2 mg/kg), and eyes received topical ocular anesthesia (0.5% proparacaine hydrochloride eye drops, Akorn Inc. Buffalo Grove, IL, USA). Next, one eye underwent intracameral injection of a 50:50 mixture of 6 μm and 1 μm microbeads (4 μL, Polybead Microspheres®, Polysciences, Inc., Warrington, PA), followed by 1 μL of viscoelastic compound (10 mg/mL sodium hyaluronate, Healon, Advanced Medical Optics Inc., Santa Ana, CA). After injection, animals were either followed for three days (3D GL) to assess transport block or for 6 weeks (6 WK GL) to assess axon loss.

2.3 IOP measurements:

To measure IOP, mice were anesthetized with either an intraperitoneal injection (ketamine (50 mg/kg), xylazine (10 mg/kg), and acepromazine (2 mg/kg), final IOP measurement prior to sacrifice) or isoflurane (for IOP reading only), using a RC2-Rodent Circuit Controller (VetEquip, Inc., Pleasanton, CA), delivering 2.5% of isoflurane in oxygen, at 500 cc/minute for inhalation. To measure IOP, a TonoLab tonometer (Icare Finland Oy, Inc., Vantaa, Finland) was used. Eyes received no topical ocular anesthesia with isoflurane, but proparacaine hydrochloride eye drops were applied to mice sedated by intraperitoneal injection of ketamine, xylazine and acepromazine. IOP was measured at the following time points: prior to injection and at 1 day, 3 days, 1 week, 2 weeks, and 6 weeks after injection (depending upon length of experiment).

2.4 Tissue Preparation:

Samples processed for APP (N=33, Mice) or axon counts (N=32, Mice) were prepped as followed. Mice were euthanized on either day 3- or week 6 after microbead injection. Firstly, the mice were anesthetized intraperitoneally (ketamine (50 mg/kg), xylazine (10 mg/kg), and acepromazine (2 mg/kg)), followed by transcardial perfusion (4% paraformaldehyde in 0.1 M phosphate buffer, Na_3PO_4, pH = 7.2) and concurrent exsanguination. Following euthanasia, the mouse eyes were enucleated with nerves attached and prepped for one of two protocols: cryopreservation (APP) or embeding in epoxy resin (axon counts).

2.5 Cryopreservation, Immunolabeling and Fluorescent Imaging:

Mouse eyes (N=33, Mice; N=66, eyes: Includes 3D GL of YLM, OLM, YB6 and OB6) were placed in increasing concentrations of sucrose solution, then finally cryopreserved in mixture of sucrose and TissueTek® O.C.T. compound solution (Sakura Finetek USA, Inc., Torrance, CA). Eyes were then cryo-sectioned at 8 μm thickness for immunofluorescent staining. Antibodies used were: rabbit anti-β amyloid precursor protein (APP) at 1:125 (Cat # 51–2700, LOT # UK294411, Invitrogen, Rockford, IL), rabbit anti-laminin at 1:1000 (Cat # L9393, MilliporeSigma, Burlington, MA), goat anti-rabbit IgG Alexa 488 secondary antibody (Cat # A-11008, Invitrogen, Eugene, OR) at 1:200 against APP primary and 1:200 against laminin primary, all sections were additionally stained with DAPI at 1:1000 (5 μg/mL, Cat # 10-236-276-001, Roche Diagnostics, Indianapolis, IN) and mounted using DAKO mounting media (Cat #S3023, Dako North America, Carpinteria, CA). All slides were masked and assigned a random identification number. The methods for imaging and quantification of APP labeling followed Korneva et al (Korneva et al, 2020). A masked investigator imaged the slides on a Plan-Apochromat 20x/0.8 M27 objective on a Zeiss confocal laser scanning microscope 710 (Carl Zeiss Microscopy, White Plains, NY) to produce 16-bit images with a 0.18 μm per pixel resolution, using independent two-channel acquisition with excitation at 488 nm for Alexa 488 and at 405 nm for DAPI. Images were stitched using ZEN 2.3 software (Carl Zeiss Microscopy, White Plains, NY) and converted to .tiff files for image analysis. All steps described above, treatment, IOP measurement, sample preparation, staining and imaging were performed on all samples of a cohort concurrently. Laminin images were taken using a Plan-Apochromat 20x/0.8 M27 objective on the same Zeiss confocal laser scanning microscope, using independent two-channel acquisition with excitation at 488 nm for Alexa 488 and at 405 nm for DAPI.

2.6 Demarcation of regions in nerve head:

APP images were imported into FIJI (ImageJ, National Institutes of Health, Bethesda, MD) and regions of interest were outlined using the polygon selection tool as previously published (Korneva et al, 2020). Regional separation was made by extending a line between the 2 ends of Bruch's membrane opening (BMO), with tissue anterior to this line denoted the preONH and posterior to it for 200 μm as the UON. The preONH region was laterally delimited by a line drawn vertically from either side of the BMO. Data from the retina included only the retinal nerve fiber layer lateral to the ONH. The UON region began at the BMO line, and extended 200 μm posteriorly. The MON region was defined as tissue from

350 μm behind the BMO line to the end of tissue in the section. The myelin transition zone, from 200 to 350 μm posterior to BMO, was excluded from analysis.

2.7 Image analysis methods:

Quantification of APP labeling was performed on both younger and older LM and B6 mice (Table 2). Selected zones from the 4 regions of interest in each image were converted to grayscale. Using MATLAB (Mathworks, Natick, MA), the distribution of the pixel intensity from each region of interest was calculated. Since axonal APP is transported through the ONH in the physiologic state, we generated metrics that capture the degree to which local, abnormally high levels of APP clumping occurred with IOP elevation as measures of axonal transport blockade. To produce these metrics, we first calculated the distribution of APP label intensity in the control (untreated) eyes of each group, including the mean, median, 97.5th and 99th percentile (%ile) values. The 97.5th and 99th%ile control values were used as benchmarks for comparison to the distribution of the 3D GL eyes. From these thresholds, we generated the following parameters: mean intensity of the pixels brighter than the 97.5th%ile of the control; mean intensity of the pixels brighter than the 99th%ile of the control, fraction of pixels brighter than the 97.5th%ile of the control and fraction of pixels brighter than the 99th%ile of the control. These metrics represent the mean and fractional intensities of pixels above the values in their respective control group benchmarks. For the 6 week glaucoma experiment, 16 YLM mice were matched by degree of IOP elevation with 16 similar aged B6 mice to compare relative optic nerve parameters.

2.8 Optic nerve axon counts:

After ocular tissue was extracted post-perfusion (N=32, Mice; N=64, eyes: Includes 6wk GL YLM and YB6), optic nerves were removed 1.5 mm behind the globe, post-fixed in 1% osmium tetroxide (OsO_4), dehydrated in ascending alcohol concentrations, and embedded in epoxy resin at 60°C for 48 hours. One μm thick cross-sections of the MON were stained with 1% toluidine blue. Low and high-power digital images were taken using a Cool Snap camera with Metamorph software (Molecular Devices, Sunnyvale, CA, USA). For each nerve, five 40 x 40 μm^2 fields were acquired, corresponding to a 9% sample of total nerve area. Masked observers edited non-axonal elements from each image, generating an axon density from the software. The average axon density/mm^2 was multiplied by the individual nerve area to estimate total axon number. The software also calculated mean axon diameter. Axon loss was calculated by comparing glaucoma eyes to the mean axon number in pooled, fellow eye nerves of each mouse strain.

2.9 Transmission Electron Microscopy:

For electron microscopy, YLM (N=4 control eyes also used in the 6 wk GL study) and YB6 (N=1 bilateral niave) mice were euthanized by exsanguination under general intraperitoneal anesthesia, followed by intracardiac perfusion for 10 minutes with 4% paraformaldehyde in 0.1 M sodium phosphate buffer (Na_3PO_4, pH = 7.2). Eyes were enucleated and post-fixed in 1% osmium tetroxide (OsO_4), dehydrated in ascending alcohol concentrations, and stained in 1% uranyl acetate in 100% ethanol for 1 hour. Tissues were embedded in epoxy resin mixture at 60°C for 48 hours. One-micron thick sections were cut and stained with 1% toluidine blue. Ultra-thin sections (~68 nm thickness) were collected on copper grids. The

grids were stained with uranyl acetate and lead citrate before being examined with a Hitachi H7600 TEM (Hitachi High Technologies, Clarksburg, MD).

2.10 Statistical Methods:

Data were compared as mean ± standard deviation or median values. Paired or unpaired t tests were used for normally distributed data and Mann Whitney tests were used for non-parametric data. Significance level was $p \leq 0.05$.

Results

3.1 Intraocular Pressure:

The baseline IOPs and experimentally elevated IOPs in the LM and B6 animal groups studied by APP transport block after 3 days of IOP elevation were statistically similar, except that the fellow, control eyes of YLM mice had slightly higher mean IOP prior to microbead injection compared to YB6 mice (Table 3 $p = 0.02$). Both strains and both ages of mice had significant IOP increase in bead-injected eyes at 1 day after injection. The mean IOP increases were not statistically different between LM and B6 mice at either age (YLM vs YB6, $p = 0.73$; OLM vs OB6, $p = 0.8$). For the 3 day APP animals, we discovered that the calibration of the tonometer was offset during 3 day measurements, but this would apply to both eyes of B6 and LM animals, so that the IOPs and their differences (Δ, glaucoma-control) could be compared (Table 3).

The mice that comprised the 6 week glaucoma experiment had no significant difference between YB6 and YLM glaucoma eyes at 1 day after bead injection and only a borderline difference after 3 days (Table 4). As has been seen with this model, the values after 1 week returned toward normal values in both groups. There were no tonometric calibration offsets in the 6 week data.

3.2 Axonal Transport Blockade

Mean pixel brightness of pixels brighter than the >97.5th%ile and >99th %ile of the control represent the extent of local APP accumulation due to IOP-induced transport block in the UON and MON, as previously reported (Korneva et al, 2020). In these regions, APP accumulation was significant in bead-injected eyes, compared to benchmarks from control fellow eyes (Supplemental Table 1, Figure 1). The degree of transport block, judged by these two measures, was statistically similar in YLM compared to YB6 (YLM control vs YB6 control, $p = 0.66$ and $p = 0.72$; YLM 3D GL vs YB6 3D GL, $p = 0.61$ and $p = 0.66$, respectively).

OB6 3D GL eyes demonstrated APP accumulation in comparison to control eyes in all 3 optic nerve regions (Figure 2, UON region). By contrast, OLM 3D GL eyes did not demonstrate increased APP accumulation compared to their controls; however, both OLM control eyes and OLM 3D GL eyes exhibited greater APP accumulation than the OB6 in every anatomical region (all p values ≤ 0.004, t tests, Supplemental Table 2).

3.3 Optic Nerve Axon Data

Control YLM had a 24% smaller nerve area and a 16.75% greater axonal density compared to YB6 controls (t tests, $p < 0.0001$ & $p \leq 0.001$ respectively, Table 4). The mean axon diameter and number of RGC axons did not significantly differ between mouse strains (t test, $p = 0.73$ & $p = 0.1$ respectively).

The 6 week bead glaucoma model produced a 12.2 % axon loss in YLM mice compared to pooled fellow eye controls ($p = 0.046$), while YB6 mice had a 18.7% axon loss in bead-injected eyes compared to controls ($p < 0.0016$; $n = 16$ per group; one sample t tests, Table 4); the percent loss in YLM did not significantly differ from that of YB6 ($p = 0.22$, Mann Whitney test). The IOP elevation at the critical early time point was matched in the two groups: e.g. mean IOP increase compared to fellow, untreated eye at first day after bead injection in B6 = 14.9 ± 5.1 mmHg, in LM = 14.6 ± 5.9 mm Hg.

3.4 Histological Features of YLM

Astrocytes normally separate ON axons from the meningeal sheaths by a limiting cellular barrier called Graefe's peripheral layer (Trivino, 1996). In the prior publication by Edwards et al. (2009), the LM mice demonstrated a failure of proper formation of the retinal ILM, allowing glial and vascular tissues to migrate into the vitreous cavity. We found a similar phenomenon in the retrobulbar optic nerve in epoxy-embedded thick section, immunolabeled cryosections, and TEM observations. Normally, astrocytes separate optic nerve axons from the pial meningeal sheath with their cell processes and their basement membrane. This prevents more direct contact between axons and the extracellular connective tissue. In several LM nerves, we found a localized absence of the pia mater and a protrusion of tissues, including astrocytes and axons, into the subarachnoid space by light microscopy (Figure 3). In these zones, the astrocytic peripheral layer was discontinuous and tissue protruded into the subarachnoid space. This tissue contained both astrocytes and axons, some of which retained their myelin sheaths and accompanying oligodendrocytes. Some of these protrusions were relatively small, while others were much larger (Figure 3D,H).

In immunolabeled, longitudinal sections of the posterior eye and ON, there was an abnormal appearance of the laminin-labeled zone that is coincident with the astrocytic basement membrane and pia mater (Figure 4). While in normal B6 mice this layer was smooth and continuous along the periphery of the ON, in LM eyes there were duplications of this laminin-containing layer (Figure 4B,E). In some cases the tissue protrusions illustrated in Figure 3 were seen to be completely outlined by this laminin labeling (Figure 4C,F).

TEM observations of B6 and LM eyes demonstrated ultrastructural differences from normal in the LM eyes in the optic nerve periphery. Normally, the ON axons are separated from the PPS and the pia mater by a continuous layer of astrocyte processes that elaborate a basement membrane containing laminin as one major component. In normal B6 eyes, the basement membrane is uniform in thickness and continuously adjacent to the astrocytes (Figure 5A). By contrast, in the UON area, LM eyes had duplications of the basement membrane that were found in whorls separated from close contact with the astrocytes (Figure 5B). In the more distal ON, there were areas of discontinuity of Graefe's peripheral layer, permiting

direct contact between ON axons and the connective tissue of the pia mater (Figure 5C,D). In an area of such discontinuity, astrocyte processes identified by their neurofilaments were seen to protrude abnormally into the subarachnoid space (Figure 5C).

4.1 Discussion

In addition to the previously reported defects in the ILM of LM mice, we demonstrate analogous abnormal features of laminin-containing structures in the optic nerve. There were localized defects in the peripheral ON, including breaks in the peripheral astrocyte layer and pia mater. These allowed astrocytes and axons to exit the normal ON path, in some cases actually reentering it more posteriorly and in others leading to clumps of tissue without viable axons in the subarachnoid space. The laminin label in these areas was either deficient or reduplicated, surrounding the aberrant tissue outside the normal boundary of the ON. There were clear areas of abnormal basement membrane in areas between astrocytes and PPS. Potentially, the failure of laminin properly to constitute the basement membrane of astrocytes led to a failure in the formation of local zones of pia mater, producing these protrusions.

We hypothesized that the laminin defect in these mice would impact the response to IOP elevation, due to the importance of laminin as a component of the basement membrane to which astrocytes are attached in the UON zone of injury. Utilizing the APP assay, there was no difference in the degree of transport block caused by elevated IOP between YLM and YB6 mice. This confirmed the reliability of our glaucoma model, as both strains showed significant transport blockage in 3D IOP elevation eyes. Likewise, OB6 mice showed similar levels of transport block to the younger groups. On the other hand, the OLM mice had greater APP accumulation than older B6 mice in both control and IOP-elevated eyes. This finding is compatible with a baseline degree of axonal transport obstruction in the older LM mice, even at normal IOP. Since this difference was not seen in comparing control YLM mice to control YB6 mice, the putative baseline transport blocking effect in OLM mice may be age dependent.

In the LM mice that underwent microbead injection in one eye, the optic nerve fiber number was somewhat lower ($p = 0.1$) than that of the B6 control eyes of the same age. Since the APP data suggest that control OLM mice have axonal transport obstruction even without IOP elevation, it is possible that this transport block leads to retinal ganglion cell and axon loss. We are presently investigating this potentially greater loss of fibers with age in LM mutants. This could indicate that the abnormality in laminin contributes to axonal injury even at normal IOP. Hypothetically, defects in laminin could represent new risk factors to explain those persons with open angle glaucoma who suffer injury at normal IOP levels. A second possible contributing feature to the lower number of axons in LM control nerves may be the failure of proper maintenance of the astrocyte barrier at the pia mater mentioned above. It is likely that if axons exited the nerve, but did not properly achieve their central target, they would not have survived embryonic or later life, leading to lower axon numbers.

The APP blockade assay carried out to assess glaucoma damage has some limitations that were noted previously (Korneva et al, 2020). There is physiological variation in baseline

APP transport and in the effect of IOP elevation on transport that necessitates study of several nerves per group. The axon loss produced by IOP elevation can vary in B6 animals from one cohort of mice to another. B6 animals, while inbred to some degree, are clearly diverse in their susceptibility to axon loss from higher IOP. This may have made it more difficult to determine a difference between the LM and B6 animals in ON damage, if a difference exists. In this report, some observations were qualitative conclusions from ultrastructural methods. Finally, while our speculation that LM may have different biomechanical responses to IOP is supported by some of the present data, we have not yet directly measured biomechanical strains resultant from higher IOP-generated stress in these mice.

Supplementary Material

Refer to Web version on PubMed Central for supplementary material.

Acknowledgments

We would like to thank Malia Edwards for providing *Lama1*^{nmf223} mutant mice and for her advice and support. We also thank Thomas V Johnson for advice and manuscript review.

This work was supported in part by PHS research grants EY 02120 (Dr. Quigley) and EY 01765 (Wilmer Institute Core grant), Research to Prevent Blindness, Inc., and by unrestricted support from Saranne and Livingston Kosberg, Mary Bartkus, and from William T. Forrester. The funders had no role in study design, data collection and analysis, decision to publish, or preparation of the manuscript.

Abreviations:

IOP	Intraocular pressure
***Lama1*^{nmf223}**	Laminin mutant (LM) mice
B6	C57BL/6J
RGC	Retinal ganglion cell
ON	optic nerve
APP	amyloid precursor protein
preONH	prelaminar optic nerve head
UON	unmyelinated optic nerve
MON	myelinated optic nerve

References:

Colognato H, Yurchenco PD. Form and function: the laminin family of heterotrimers. Dev Dyn. 2000; 218:213–234. [PubMed: 10842354]

Cone FE, Steinhart MR, Oglesby EN, Kalesnykas G, Pease ME, Quigley HA. The effects of anesthesia, mouse strain and age on intraocular pressure and an improved murine model of experimental glaucoma. Exp Eye Res. 2012;99(1):27–35. doi:10.1016/j.exer.2012.04.006 [PubMed: 22554836]

Cone-Kimball E, Nguyen C, Oglesby EN, Pease ME, Steinhart MR, Quigley HA. Scleral structural alterations associated with chronic experimental intraocular pressure elevation in mice. Mol Vis. 2013;19:2023–2039. [PubMed: 24146537]

Edwards MM, Mammadova-Bach E, Alpy F, et al. Mutations in Lama1 Disrupt retinal vascular development and inner limiting membrane formation. J Biol Chem. 2009; 285:7697–7711.

Falk M, Ferletta M, Forsberg E, Ekblom P. Restricted distribution of laminin alpha1 chain in normal adult mouse tissues. Matrix Biol. 1999 Dec;18(6):557–68. doi: 10.1016/s0945-053x(99)00047-5. [PubMed: 10607917]

Gelman S, Cone FE, Pease ME, Nguyen TD, Myers K, Quigley HA. The presence and distribution of elastin in the posterior and retrobulbar regions of the mouse eye. Exp Eye Res. 2010; 90:210–215. 10.1016/j.exer.2009.10.007 [PubMed: 19853602]

Hernandez MR. The optic nerve head in glaucoma: role of astrocytes in tissue remodeling. Prog Ret Eye Res. 2000; 19:297–321.

Howell GR, Libby RT, Jakobs TC, Smith RS, Phalan FC, Barter JW et al. Axons of retinal ganglion cells are insulted in the optic nerve early in DBA/2J glaucoma. J Cell Biol. 2007; 179:1523–1537. 10.1083/jcb.200706181 [PubMed: 18158332]

Jones HJ, Girard MJ, White N, Fautsch MP, Morgan JE, Ethier CR, et al. Quantitative analysis of three-dimensional fibrillar collagen microstructure within the normal, aged and glaucomatous human optic nerve head. J R Soc Interface. 2015; 12: 20150066. 10.1098/rsif.2015.0066 [PubMed: 25808336]

Kohno T, Sorgente N, Ishibashi T, Goodnight R, Ryan SJ. Immunofluorescent studies of fibronectin and laminin in the human eye. Invest Ophthalmol Vis Sci. 1987; 28:506–514. [PubMed: 3549611]

Korneva A, Schaub J, Jefferys J, et al. A method to quantify regional axonal transport blockade at the optic nerve head after short term intraocular pressure elevation in mice. Exper Eye Res. 2020; 196:108035. doi: 10.1016/j.exer.2020.108035. [PubMed: 32353427]

Morrison JC, L'Hernault NL, Jerdan JA, Quigley HA. Ultrastructural location of extracellular matrix components in the optic nerve head. Arch Ophthalmol. 1989; 107:123–9. [PubMed: 2910271]

Morrison JC. Integrins in the optic nerve head: potential roles in glaucomatous optic neuropathy. Trans Am Ophthalmol Soc. 2006; 104:453–477. [PubMed: 17471356]

Pijanka JK, Spang MT, Sorensen T, Liu J, Nguyen TD, Quigley HA, et al. Depth-dependent changes in collagen organization in the human peripapillary sclera. PLoS One. 2015; 10: e0118648. 10.1371/journal.pone.0118648 [PubMed: 25714753]

Quigley HA, Addicks EM, Green WR, Maumenee AE. Optic nerve damage in human glaucoma. II. The site of injury and susceptibility to damage. Arch Ophthalmol. 1981; 99:635–649. 10.1001/archopht.1981.03930010635009 [PubMed: 6164357]

Quigley HA, Addicks EM. Chronic experimental glaucoma in primates. II. Effect of extended intraocular pressure elevation on optic nerve head and axonal transport. Invest Ophthalmol Vis Sci. 1980; 19:137–152. [PubMed: 6153173]

Quigley HA, Brown A, Dorman-Pease ME. Alterations in elastin of the optic nerve head in human and experimental glaucoma. Br J Ophthalmol. 1991; 75:552–557. 10.1136/bjo.75.9.552 [PubMed: 1911659]

Quigley HA. Understanding glaucomatous optic neuropathy: The synergy between clinical observation and investigation. Annu Rev Vis Sci. 2016; 2:235–254. [PubMed: 28532352]

Quillen S, Schaub J, Quigley H, Pease M, Korneva A, Kimball E. Astrocyte responses to experimental glaucoma in mouse optic nerve head. PLoS One. 2020;15: e0238104. [PubMed: 32822415]

Sun D, Lye-Barthel M, Masland RH, Jakobs TC. The morphology and spatial arrangement of astrocytes in the optic nerve head of the mouse. J Comp Neurol. 2009; 516:1–19. 10.1002/cne.22058 [PubMed: 19562764]

Triviño A, Ramírez JM, Salazar JJ, Ramírez AI, García-Sánchez J. Immunohistochemical study of human optic nerve head astroglia. Vision Res. 1996; 36:2015–28. doi: 10.1016/0042-6989(95)00317-7. [PubMed: 8776468]

Zhang K, Johnson TV. The internal limiting membrane: Roles in retinal development and implications for emerging ocular therapies. Exp Eye Res. 2021; 206:108545. doi: 10.1016/j.exer.2021.108545. [PubMed: 33753089]

Zhong Y, Wang J, Luo X. Integrins in trabecular meshwork and optic nerve head: Possible association with the pathogenesis of glaucoma. Biomed Res Int. 2013; 2013:202905. [PubMed: 23586020]

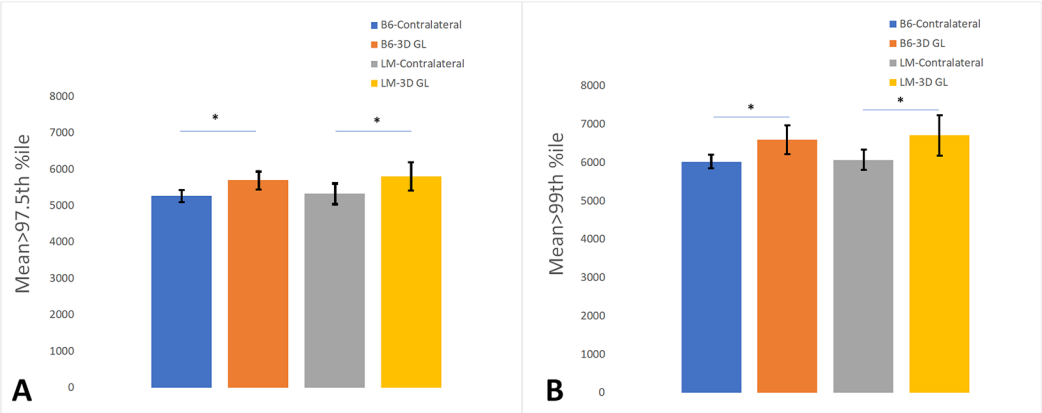

Figure 1: Transport Blockade Data in the UON Region, Younger C57BL/6J and Laminin Mice

Amyloid precursor protein (APP) intensity values for mean brightness over the naïve control 97.5^{tho}%ile (A) and 99^{tho}%ile (B) for control and 3-day (3D) glaucoma (GL) eyes in younger C57BL/6J (B6) and younger Laminin Mutant (LM) animals. Both B6 and LM GL groups have significantly higher axonal transport block by these measures (* indicates $p \leq 0.01$).

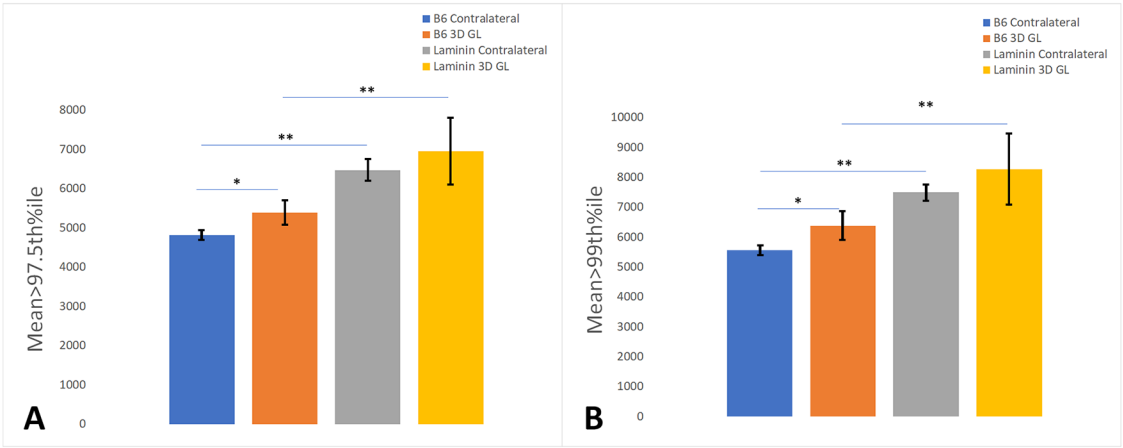

Figure 2: Transport Blockade in UON Region, Older C57BL/6 and Laminin Mutant Mice

Mean amyloid precursor protein (APP) intensity of pixels with brightness greater than the 97.5th (A) and 99th%iles (B) of bright pixels in the naïve nerves for control and glaucoma (GL) eyes in older C57BL/6J (B6) and older laminin mutant (LM) animals. Older B6 GL eyes show significant transport block compared to their control nerves (*indicates $p \leq 0.001$). Older LM GL group does not significantly differ in transport block from their control nerves ($p = 0.13$ & $p = 0.08$), but both older LM GL and their control nerves have more transport block than the corresponding older B6 groups by both measures (** indicates $p \leq 0.004$).

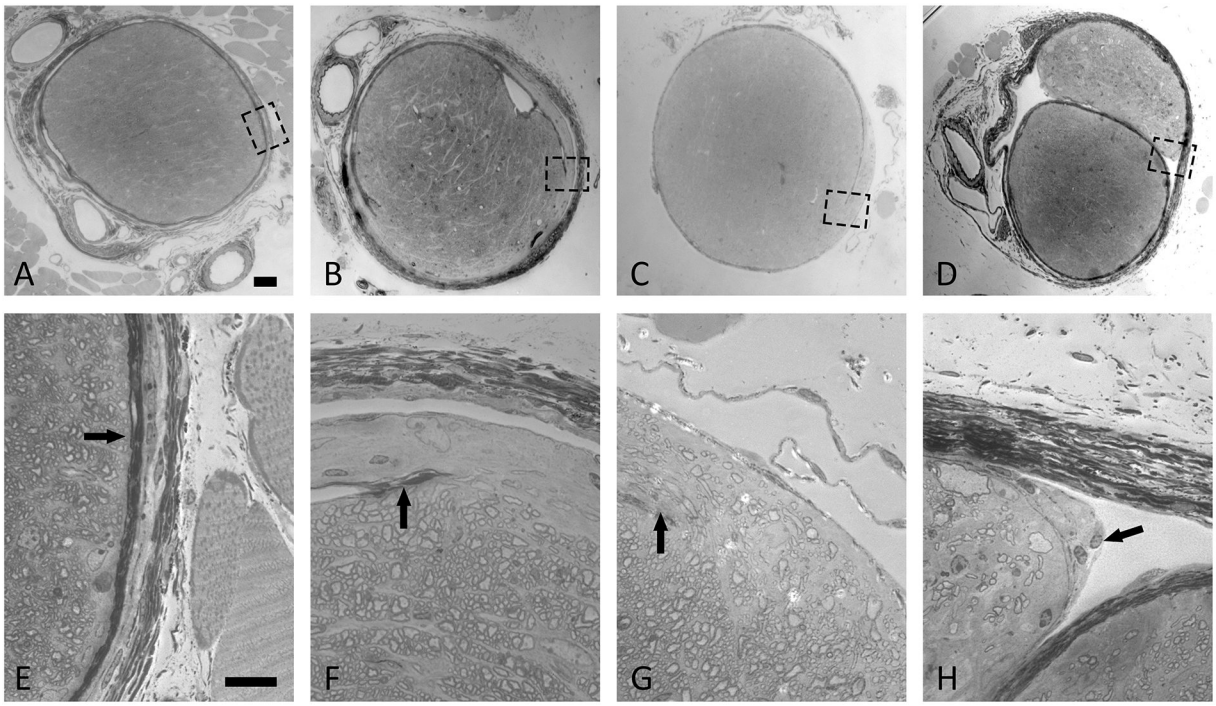

Figure 3: Myelinated optic nerve cross-sections of laminin mutant eyes

Epoxy cross-sections of young C57BL/6J (B6, A, E) and laminin (YLM, B-D and F-H) optic nerves. Low magnification images (A-D) and higher magnification images of each nerve (E-H). A, E: Control B6 nerve demonstrates intact peripheral astrocytic layer underlying pia mater (dark zone, arrow). Nerves from younger LM eyes (E-H) show several zones of defective peripheral astrocyte layer and local discontinuity in pia mater. B-F: defect in peripheral astrocytes and pia mater structure (arrow) with cells typical for astrocytes and oligodendrocytes present in the subarachnoid space. C, G: Defect in pia allows myelinated axons to exit normal nerve and course into subarachnoid space (arrow). D, H: Aberrant axons and associated tissue are separate from the main nerve and partially encased by a new pia-like structure (arrow). (Toluidine blue stain). Scale Bar A-D= 10 μm, Scale Bar E-H = 20 μm.

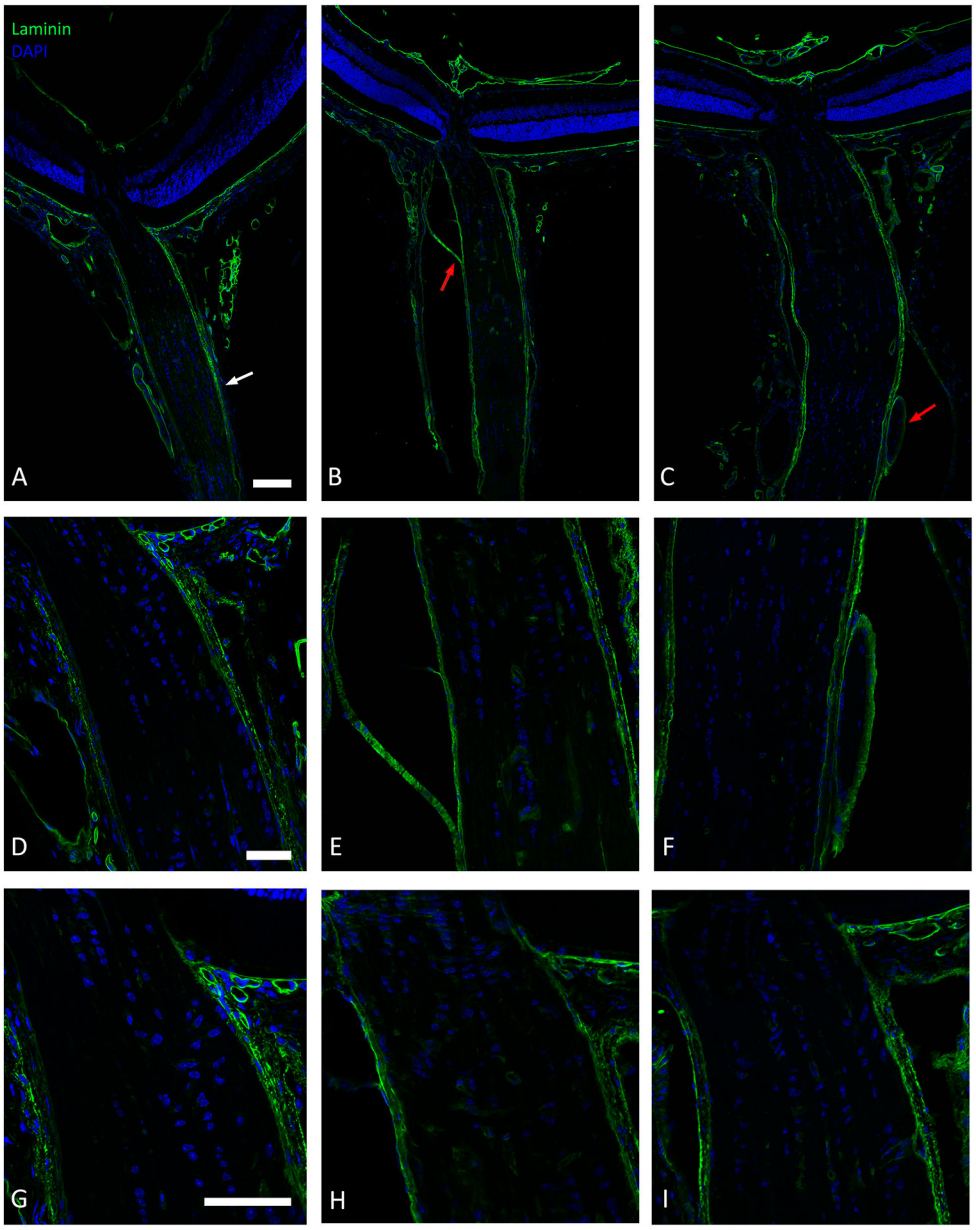

Figure 4: Laminin immunolabeling of laminin mutant eyes

Younger C57BL/6J (YB6; A, D, G) and Younger Laminin Mutant (YLM; B-C, E-F, H-I) longitudinal optic nerve sections labeled with anti-laminin antibody (green) and DAPI (blue). A, D: YB6 nerve with typical, intact pia (white arrow) and unaltered axon bundles. B, C: YLM nerves with duplicated pia parallel to the nerve (red arrows), found both at the unmyelinated nerve (B) and at the myelinated nerve (C). D, E, F: Magnified views of of normal B6 nerve (D), and of pial duplications in B, C (E, F). G, H, I: Higher power views of the glial lamina region in YB6 (G) and YLM (H,I). Scale Bar A-C = 100 μm, Scale Bar D-F = 50 μm, Scale bar G-I = 50 μm.

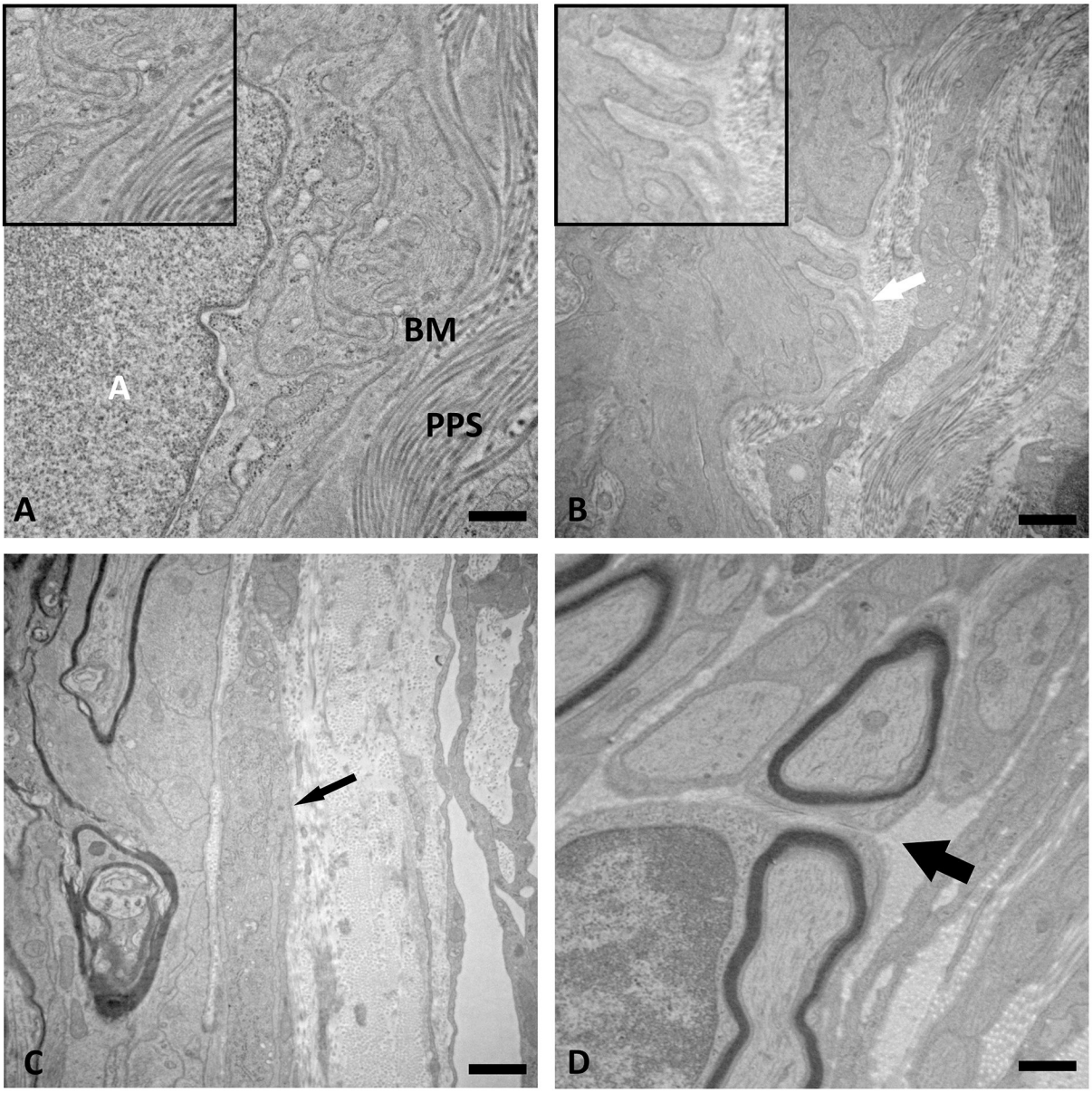

Figure 5: Transmission electron micrographs of B6 and Laminin mutant optic nerve

Younger B6 (YB6; A) and Younger Laminin Mutant (YLM; B-D) images of border zone between optic nerve and peripapillary sclera (PPS) by transmission electron microscopy. A: Normal B6 optic nerve shows astrocyte (white A) and astrocyte processes separating nerve tissue from PPS (Inset has enlarged view of the normal basement membrane (BM)). B: Abnormal duplication of basement membrane of astrocytes in border area of unmyelinated optic nerve adjacent to PPS (white arrow and inset). C: Reduplication of astrocytes processes into the pia mater (black arrow). D: In YLM optic nerve, an area of discontinuous astrocyte and pia mater coverage allows direct exposure of myelinated nerve fibers to collagenous connective tissue (thick black arrow). Scale Bar A-D = 1 μm.

Table 1:

Enumeration of mice used

Strain	Age	Sex	Studies, Abbreviation	Sample Mice
C67BL/6Jp (B6)	Younger (Y), Older (O) Younger (Y) Younger (Y)	M + F M + F F M	APP analysis, 3D GL APP analysis, 3D GL Axon Counts, 6Wk GL Bilateral naïve, TEM	N= 5 N= 7 N=16 N=1
Laminin (LM)	Younger (Y), Older (O) Younger (Y)	M + F M + F M + F	APP analysis, 3D GL APP analysis, 3D GL Axon Counts, 6Wk GL, TEM	N=12 N= 9 N=16

Some data from B6 samples (YB6, 6 Wk GL Axon Counts, N=16) were previously published. (Cone-Kimball et al, 2013)

Table 2:

Numbers of mouse eyes in APP study groups

	Group Title	N*	Treatment	Abbreviation
Cohort #1	Young B6 Glaucoma	5	3-day IOP elevation	YB6-3D GL
	Young B6 Cotnrol	5	Contralateral eye, No IOP elevation	YB6-Control
	Young Laminin Mutant Glaucoma	12	3-day IOP elevation	YLM-3D GL
	Young Laminin Mutant Control	12	Contralateral eye, No IOP elevation	YLM- Control
Cohort #2	Old B6 Glaucoma	7	3-day IOP elevation	OB6-3D GL
	Old B6 Control	7	Contralateral eye, No IOP elevation	OB6-Control
	Old Laminin Mutant Glaucoma	9	3-day IOP elevation	OLM-3D GL
	Old Laminin Mutant Control	9	Contralateral eye, No IOP elevation	OLM- Control

*N= number of eyes.

Table 3:

3D GL Intraocular Pressure Data

	N	Control IOP Pre-Injection	GL IOP Pre-Injection	Control Day 1 IOP	GL Day 1 IOP	Δ (GL- C) Day 1	Control Day 3 IOP	GL Day 3 IOP	Δ (GL - C)Day 3
YB6	5	12.8 ± 0.4	11.8 ± 1.3	9.4 ± 2.9	28.6 ± 3.8^{+}	19.2 ± 5.4	8.4 ± 0.5	19 ± 5.2	10.6 ± 5.3
YLM	12	12.9 ± 2.7	15.7 ± 3.2	13.1 ± 3.7	29.4 ± 4.5^{+}	16.3 ± 6.2	11.8 ± 3.1	18.5 ± 3.9	6.8 ± 3.8
YB6 vs YLM p values		0.926	**0.02**	0.067	0.726	0.384	**0.033**	0.828	0.107
OB6	7	11.0 ± 2.4	12.9 ± 2.0	12.3 ± 3.2	29.3 ± 5.0^{+}	17 ± 4.9	9 ± 2.2	20.4 ± 5.8	11.4 ± 4.3
OLM	9	13.6 ± 3.5	13.0 ± 3.4	14.9 ± 4.4	28.8 ± 3.1^{+}	13.9 ± 5.6	10.8 ± 3.2	15.8 ± 4.2	5 ± 5.1
OB6 vs OLM p values		0.119	0.923	0.208	0.804	0.268	0.236	0.083	**0.018**

Data are mean ± standard deviation. IOP in mm Hg. Δ, glaucoma (GL) – control (C). P-values, t-test, $p \leq 0.05$. + = statistical differences between mean glaucoma (GL) eyes on day 1 compared to age and strain matched pre-injection IOPs, $p \leq 0.0001$, t tests.

Table 4:

6Wk GL Intraocular Pressure Data

	N	Control eyes	GL eyes	Control eyes	GL eyes	Control eyes	GL eyes	Control eyes	GL eyes	Control eyes	GL eyes	Control eyes	GL eyes
		IOP Pre-Injection	IOP Pre-Injection	Day 1 IOP	Day 1 IOP	Day 3 IOP	Day 3 IOP	Week 1 IOP	Week 1 IOP	Week 2 IOP	Week 2 IOP	Week 6 IOP	Week 6 IOP
YB6	16	10.9 ± 1.8	10.5 ± 2.9	13.9 ± 2.2	28.8 ± 5.8	13.9 ± 2.2	25.8 ± 7.2	16.3 ± 2.4	24.8 ± 8.9	13.9 ± 1.8	16.8 ± 9.2	10.8 ± 2.1	12.5 ± 5.7
YLM	16	13.4 ± 2	13.6 ± 2.6	12 ± 3.7	26.6 ± 5.4	17.6 ± 4	20.9 ± 5.8	18.6 ± 1.9	19.5 ± 6.6	16.7 ± 2.3	16.4 ± 5.6	9.8 ± 2.1	9.9 ± 2.6
YB6 vs YLM p values		**0.001**	**0.004**	0.087	0.290	**0.002**	**0.045**	**0.005**	0.066	**0.001**	0.890	0.188	0.104

Data are mean ± standard deviation. IOP in mm Hg.

Table 5:

Optic Nerve Axon Data

	N	Control Density	Control Area	Control # Fibers	Glaucoma Density	Glaucoma Area	Glaucoma # Fibers	% Axon Loss
YLM	16	591,734 ± 73,438	0.068 ± 0.009	40,191 ± 5,876	552,164 ± 133,108	0.064 ± 0.009	35,291 ± 9,003	12.2 ± 22.4%
YB6	16	492,594 ± 82,982	0.090 ± 0.009	44,048 ± 7,143	455,047 ± 88,238	0.079 ± 0.013	35,826 ± 8,610	18.7 ± 19.5%
t-test		**p = 0.001**	**p < 0.0001**	p = 0.1	**p = 0.02**	**p < 0.001**	p = 0.86	p = 0.22 *

Density = axons/mm^2. Area units = mm^2.

* = Mann Whitney test.